

Gas, Dust, and Young Stars in the Outer Disk of M 31

Jean-Charles Cuillandre

Canada-France-Hawaii Telescope, PO Box 1597, Kamuela HI 96743

James Lequeux

Observatoire de Paris, 61 Avenue de l'Observatoire, 75014 Paris, France

Ronald J. Allen

Space Telescope Science Institute, 3700 San Martin Drive, Baltimore, MD 21218

Yannick Mellier and Emmanuel Bertin

*Institut d'Astrophysique de Paris, 98 bis, bd Arago, 75014 Paris, France; and
Observatoire de Paris, 61 Avenue de l'Observatoire, 75014 Paris, France*

ABSTRACT

Using the Canada-France-Hawaii Telescope we have obtained deep high-resolution CCD images in V and I of a $28' \times 28'$ field in the outer disk of M 31 at $\approx 116'$ from the center along the major axis to the south-west, and covering a range of projected galactocentric distance from about 23 to 33 kpc. The field was chosen to correspond with extended HI features recorded near the HI edge of the galaxy.

The many tens of thousands of objects detected in this large field have been classified using an automatic algorithm which distinguishes unresolved from resolved structures and provides photometry on them. For the most part the unresolved objects are stars in M 31. The V-I colors of these stars are highly correlated with the column density of HI in the field. Assuming a Galactic extinction law, this yields a minimum extinction/atomic-gas ratio about 1/3 of that in the Solar neighbourhood. The ISM in this outer disk of M 31 therefore contains substantial amounts of dust.

We have identified a population of B stars in the field whose distribution is also well correlated with the extended HI distribution. Evidently, star formation is both ongoing and wide spread in the outer disk of M 31. According to the current view of the star formation process, molecular gas is therefore also expected to be present.

The objects classified as “resolved” turn out to be a mix of background galaxies and overlapping images of foreground stars in M 31. The counts and colors of the slightly-resolved objects in these ground-based CCD images therefore cannot be used for a reliable determination of the total extinction and reddening by the interstellar medium in M 31. However, the larger background galaxies are easily recognizable, and their surface density above a specific magnitude limit is anti-correlated with the HI column density, confirming that a relatively large amount of extinction is closely associated with the HI gas.

Subject headings: galaxies: individual: M 31 — galaxies: ISM — galaxies: star formation — ISM: dust, extinction: stellar populations

1. Introduction

How “primordial” is the interstellar gas in the far outer parts of galaxies? Does this gas show any signs of metal enrichment? How much dust is there in the outskirts of galaxies? Is there any evidence for substantial quantities of dark matter in the form of H₂ in these regions? The answers to these questions are relevant to our understanding of galaxy formation and evolution and the chemical enrichment of the interstellar medium over time. However, the low densities and faint radiation fields in the outskirts of galaxies make it difficult to detect dust in the interstellar medium (ISM) there.

There are strong incentives to attempt a detection and quantification of the amount of dust present in the outskirts of galaxy disks. Large amounts of dust might indicate indirectly the presence of large quantities of otherwise undetectable molecular hydrogen. Cold molecular hydrogen has been suggested as a possible component of dark matter in the disks and even the halos of spiral galaxies. It is not clear that this H₂ would have to be associated with H I, so that dust uncorrelated with H I might indicate the presence of H₂. On the other hand, when dust is observed to be correlated with H I, one can hope to determine the dust-to-gas ratio and, indirectly, the metallicity of the gas (e.g. Bouchet et al. (1985)). This may offer the best way to determine the metallicity in the outer regions of galactic disks, where there are generally no bright H II regions.

Hodge (1974) used visual counts of galaxies to map the extinction in the SMC, comparing this to the H I in order to obtain the gas/dust ratio. MacGillivray (1975) did the same work in a more detailed way and found regions of high absorption at the edges of the SMC. Using these results, Lequeux (1994) suggested that a large amount of molecular hydrogen exists in the outer parts of the SMC. The colors of background galaxies were used by Zaritsky (1994), and later by Lequeux et al. (1995) to search for dust in the halos of galaxies. The first convincing results on disk galaxies were obtained by González et al. (1998) using bright background galaxies identified by their appearance and colors on HST images of a nearby foreground galaxy. González et al. (1998) obtained the reddening from galaxy colors and the extinc-

tion from galaxy counts, using a method of comparison with *synthetic fields* in order to calibrate the effects of confusion on the search and classification algorithms. The high angular resolution of HST was crucial to the success of this method. However, careful visual examination of all candidate galaxies was also required, and this method is therefore quite time-consuming.

In this paper, we discuss the reddening and extinction in a field far out in the disk of M 31, based on observations of M 31 stars and of background galaxies. A by-product of this observation is the photometry of a large number of stars, from which high-quality color-magnitude (C-M) diagrams can be constructed, as well as maps of different categories of stars. Section 2 describes briefly the observations and the calibrations. In §3 we describe the analysis of the data, and in §5.2 we determine a lower limit to the extinction from the C-M diagrams of the stars. Section 6 discusses the distribution on the sky of relatively bright background galaxies and their extinction and reddening. In §7 we show the locations of young blue stars found in the field and discuss the relation of these young stars to the H I. Our conclusions are summarized in §8.

2. The Data

2.1. Observations

We observed a field of $28' \times 28'$ with the large-format UH8K CCD mosaic at the prime focus of the Canada-France-Hawaii Telescope. The field is centered at $00^{\text{h}}36^{\text{m}}66^{\text{s}}$, $+39^{\circ}48'50''$, J2000.0 and located $\approx 116'$ from the center of M 31 along the major axis to the south-west¹, covering a range of projected galactocentric distance from approximately 23 to 33 kpc. This region is at the extreme limit of the visible disk of the galaxy on the SW side, with $\mu_B \gtrsim 26.5 \text{ mag arcsec}^{-2}$, and extends from 4 to 5.7 times the disk scale length in the B band (Innanen 1982; Walterbos & Kennicutt 1988). It also includes the outer boundary of the H I disk as observed by Newton & Emerson (1977). Figure 1 is a sketch of the location of our full UH8K CCD field of view on the image of M 31.

¹We use the conventional distance of 690 kpc for M 31, in which case $1' = 200.7 \text{ pc}$ along the major axis of the galaxy. A very recent estimate puts M 31 at a distance of 890 kpc (Feast et al. 1999), in which case $1' = 258.9 \text{ pc}$.

The observations were made in October 1995 with a mosaic camera consisting of 8 CCDs, each 2048×4096 pixels, arranged into a 4×2 array totalling 8192×8192 pixels. The pixel size corresponds to $0.206''$ on the sky. Unfortunately, one of the eight CCDs (the chip in the north-west corner) was not of the same quality as the others, and we have ignored this part of the field. The final UH8K field is shown in Figure 2 with a grid overlaid to show the disposition of the eight CCD chips.

Our observations consisted of a series of 20-minute exposures collected over 4 nights at the telescope, 16 in I and 17 in V. Of these, 10 in I and 11 in V were of good photometric and seeing quality, giving total exposure times of 200 and 220 minutes, respectively. The filter responses are uniform over the whole field and are close to the Cousins system. The 8 thick CCDs come from a similar batch and have the same response, which is uniform across the chip. The individual exposures were slightly shifted in position with respect to each other in order to fill in the gaps between the individual chips and to permit the identification of bad pixels and cosmic rays. The separate exposures were then regridded onto a common $0.206''$ grid, recentered, and averaged after clipping aberrant pixels. This procedure effectively eliminated bad pixels and pixels affected by the impacts of cosmic rays, while retaining the correct photometry. The point spread function (PSF) on the combined exposures is $\approx 0.70''$ FWHM in both bands.

At the time these observations were made (October 1995) the capabilities available in the standard data reduction systems such as IRAF and IDL were inadequate to cope either with the volume or with the mosaic format of the UH8K CCD camera data. Furthermore, the UH8K camera is only one step in a larger program of wide-field CCD imaging at the CFHT aimed at commissioning a camera with $18,000 \times 20,000$ pixels in 2002 (MegaCam, Boulade et al. (1998)). A new image processing system (FLIPS, FITS Large Images Processing Software) was therefore developed to deal efficiently with the new large mosaic data sets (Cuillandre 2001).

2.2. Calibration

Each CCD was separately calibrated by observing standard stars in the SA 113 field (Landolt

1992). These stars span a reasonable range in color, so that color equations can be computed. The zero points and colors were obtained by using a single setting of the mosaic camera on the field, providing different SA 113 stars on each CCD. Flat-fielding was done with a library “superflat” resulting from the combination of all the available observations made with this mosaic camera in the week preceding our M 31 observing run. However, some small discrepancies remain (maximum 4%) owing to instabilities in the CCDs and to small errors in the color equation. A final correction was made by adding a small constant to each CCD in order to align the V-I colors of the pixels along neighboring edges of each CCD. The final internal standard error for each CCD on the calibration stars is 0.05 mag in V and 0.04 mag in I, while the standard deviations between CCDs are 0.02 and 0.04 mag, respectively.

As an example of the detailed image characteristics we show in Figure 3 a portion of the final averaged V image from CCD3. This image illustrates the high density of M 31 stars, as well as showing several bright galaxies.

3. Image Analysis

We have carried out an automatic classification of objects in the entire field using a recent version of the algorithm SExtractor (Bertin & Arnouts 1996). The task PSFEx was used to identify stellar objects on the image and to perform stellar photometry. “Stars” were defined as objects with $\text{FWHM} < 1.1''$ (the PSF is estimated to be $0.70''$) and ellipticity < 1.2 . “Galaxies” were defined as objects with $\text{FWHM} > 1.5''$ and any ellipticity; the task MAGAUTO in SExtractor was used for photometry of the galaxies. The result is a catalog of stars and a catalog of candidate galaxies with V and I magnitudes.

In total, more than 170,000 objects were catalogued in two colors on 7 of the 8 UH8K CCD chips. In Figure 5a we show the histograms of the magnitudes of all objects catalogued on a representative subfield of area 100 arcmin^2 from CCD1 on the final image. These histograms show that the counts of detected objects rise smoothly up to the magnitude limits adopted, and that our sample is therefore essentially complete for $V < 25.4$, $I < 24.4$. In Figure 5b we show the histogram of

the widths (FWHM) of objects in the same sub-field, confirming a high degree of completeness in our sample for $\text{FWHM} > 0.7''$ as well as justifying our choice of the size limit for stars ($\text{FWHM} < 1.1''$). Unfortunately, as we shall see in the next section, the “shoulder” in this histogram from roughly $1.4''$ to $2.3''$ is coming mostly from overlapping star images and not from faint background galaxies.

4. Counts of Small Field Galaxies

We constructed C–M diagrams for those objects classified as “galaxies” in various parts of our M 31 field, and compared the results to data obtained in other programs with the same mosaic camera on “blank” fields located far from any nearby galaxy. We first describe the results on the blank field.

4.1. Galaxies in a “blank” field

The blank field we have used for comparison with M 31 is in SA 57 near the North Galactic Pole (Majewski et al. 1994). It was observed for several hours both in V and I for another project, using the same combination of instrumentation as we have used for M 31. These data were also reduced, combined, and calibrated by one of us (J.C.) with the same procedures we have used for M 31. A portion of the final averaged image field in V is shown in Figure 4.

Figure 6 shows a C–M diagram for all blank-field galaxies in CCD3 of the UH8K mosaic. The numbers along the left side of the plot give the number of galaxies in the relevant magnitude interval. In Table 1 we collect some data for counts and colors of blank field galaxies which will be useful later. Above the completeness limit of $V < 24.75$, there are 2025 *bona fide* galaxies larger than $1.5''$ in this $7.03' \times 14.06'$ field.

4.2. “Galaxies” in the M 31 field

The comparison of our results on objects classified as galaxies in the M 31 field with the blank field described above shows that our “galaxies” are severely contaminated by confusion from overlapping images of stars in M 31, since there are significantly more “galaxies” per unit area in our M 31 field than there are in blank sky fields. For instance, in the part of the C–M diagram limited

by $V < 24.75$ where incompleteness is not a serious problem, the classification algorithm finds ≈ 6000 candidate galaxies per CCD frame in M 31, whereas the same algorithm finds only 2025 *bona fide* galaxies larger than $1.5''$ in the same area of the blank field C–M diagram (Figure 6). Under these conditions, it is clearly hopeless to try to use counts and colors of faint background galaxies in order to determine reddening and extinction in our M 31 field.

However, we shall see that the C–M diagrams for the stars are very clean (e.g. Figures 8a and b to be described below), and can be used to determine at least a *lower limit* to the total opacity through the outer disk of M 31. Also, analogous to the method used by González et al. (1998), bright background galaxies are large enough to be recognized unambiguously in our field and are not too numerous to count visually, so that estimates of variations in number density and colors of these bright galaxies can be determined.

5. C–M Diagrams of the Stars in M 31

As a first comparison of the stellar color–magnitude (C–M) diagrams in gas-rich and gas-poor parts of the field, we have defined two regions which are representative of the lowest and highest HI content. Figure 7 shows these areas with respect to the HI contours. These regions have the same area on the sky, 70 arcmin^2 .

Figure 8b shows a diagram of V vs. V–I for the faint-HI area. The boxes drawn on the Figure show the approximate locations of B stars and Red Giants (RG) expected in M 31 for a distance modulus of 24.19 mag, corresponding to our adopted distance of 690 kpc. Figure 8a shows the corresponding C–M diagram for the region of high HI column density. This region includes the sky within the 4th brightest contour on the HI data, i.e. average HI columns in excess of $N(\text{HI}) = 1.1 \times 10^{21} \text{ HI atoms cm}^{-2}$. This figure differs in two important ways from the C–M diagram in the low-HI areas: First, the bulk of the stars appear to be both slightly *redder* and slightly *fainter*, indicating the presence of obscuring dust; and second, *a population of B stars has appeared*, indicating recent star formation.

We have made a rough estimate of the “reddening law” in this part of M 31 by determining

visually the shift in V and $V-I$ from Figure 8b to Figure 8a. The process is sketched in Figure 9. The approximate result is $E(V-I) \approx 0.17$, $A_V \approx 0.35$, so that $E(V-I)/A_V \approx 0.5$, which is very close to the (more precise) value of 0.52 for dust in the Galaxy (Savage & Mathis 1979).

We note that our estimates of star counts in M 31 are contaminated by unresolved background galaxies. However, this effect is small; for $V < 24.75$ there are ≈ 2000 galaxies per CCD frame in the reference field we have taken far from any foreground galaxies, as described in §4.1. But in our M 31 fields there are $\gtrsim 20,000$ stars per CCD frame at this magnitude level. The contamination by unresolved background galaxies in Figures 8a and 8b is therefore negligible.

5.1. Color variations of the stars

In order to quantify the variations in the colors of the stars with location over this part of M 31, we split the entire image up into small square sub-areas of size 340×340 pixels = $1.167' \times 1.167' = 1.36$ arcmin 2 which we call a “superpixel”, large enough to contain a sufficient number of stars for reasonable statistics (about 230 stars within the magnitude and color limits adopted), but small enough to show variations on the arcminute scale over the image. For each superpixel we build the histogram of $V-I$ colors. The rms dispersion σ is measured, and the histogram clipped at 2σ in order to minimize the effect of the histogram wings which are contaminated by objects with peculiar colors and affected by incompleteness at the faint magnitudes. We then calculate the average color $\langle V-I \rangle$ for the remaining part of the histogram². Finally, to ensure a reasonable degree of completeness and to avoid objects not likely to be M 31 stars, we have limited our analysis of the superpixel C–M diagrams to the range $V < 25.4$, $20.5 < I < 24.4$. These cutoffs were chosen to keep the sample complete over the whole mosaic, although the most constraining chip is CCD2 in

²Of course the colors of individual stars depend on their magnitudes as well, which is clear from the C–M diagram in e.g. Figure 8a. However, we care only about the variation in *average* colors with position in the field. Since the slope of the C–M relation for Red Giants is relatively constant over the field (and the same as that in many other fields both in M 31 and outside of it), our results on the average colors above our magnitude limit are not likely to be affected.

the upper left of the mosaic closest to the main body of M 31. For the analysis of average colors of the old disk stars we also want to avoid including blue stars, since their density appears to vary over the image (cf. §7); for this analysis we therefore limit the range of object colors to $0.5 < V-I < 4$.

In Figure 10 we show representative C–M diagrams for two superpixels, one in an HI-rich region, and the other in an HI-poor region, along with their accompanying histograms. The 2σ clip levels are shown as vertical lines in the histograms, and the short horizontal arrows are 1σ in length and anchored in a large dot showing the mean color. Compared to the histogram of the HI-poor area, the histogram in the HI-rich region has about the same shape and location on the blue side, but is noticeably wider on the red side, with two secondary peaks extending the distribution about 0.5 mag further to the red. For the present purposes we use only the shift in the mean color, but we note that the shape of the histogram in the HI-rich area suggests a clumpy distribution of obscuration, on length scales smaller than the ≈ 200 pc size of a superpixel, and with opacity values up to two or more times the mean opacity over the superpixel.

5.2. The correlation of stellar $\langle V-I \rangle$ with $N(\text{HI})$

A map of the superpixel $\langle V-I \rangle$ for $V < 25.4$, $20.5 < I < 24.4$ was constructed and then smoothed to 3×5 superpixels = $3.5' \times 5.85'$, approximately the same angular resolution as the HI map of Newton & Emerson (1977) ($3.6' \text{ EW} \times 5.8' \text{ NS FWHM}$)³. The two maps are shown superimposed in Figure 11, where the contours represent $N(\text{HI})$ and the grey scale $\langle V-I \rangle$. A good correspondence appears to exist between the reddest superpixels and the highest column densities of HI. This indicates not only that there is dust mixed in with the HI in these outermost parts of M 31, but that the dust is of such a nature as to cause at least some measurable additional reddening of the light from the stars embedded in it. The reddening deduced here is, of course, only a lower

³Note that the map shown here in Figure 11 has been corrected for the primary beam response of the radio telescope used to produce it, contrary to the maps published in the original paper by Newton & Emerson (1977).

limit to the total reddening through the disk of M 31, since some fraction of the stars we are using will be in front of the absorbing material.

In order to determine the amount of dust extinction present in the H I cloud in Figure 11 we must make some assumption about the reddening law connecting the excess reddening $E(V-I)$ of starlight with the extinction A_V . For the Galaxy this is $E(V-I)/A_V = 0.52$ (Savage & Mathis 1979). In section 5 we have estimated this value to be ≈ 0.5 for our M 31 field. However, we prefer to use the more accurate Galactic value, since our determination is only approximate. This means that extinction e.g. at V moves the representative points in the V, V-I diagram not at constant V, but along reddening lines of slope $E(V-I)/A_V = 0.52$ (see e.g. Figure 9). This introduces a small correction since the true $E(V-I)$ is therefore only about 90% of that obtained by considering the change in $\langle V - I \rangle$ as a function of position at constant V. We have made this correction in what follows.

A further potential problem is the fact that V-I also depends on the metallicity of the stars as well as on the characteristics of the intervening dust. We do not expect to find much change in metallicity over the small part of the M 31 disk appearing in our image, but the V-I color will become bluer when one enters the halo. It is of course not possible to exclude completely the contribution of halo stars in each superpixel, but we can try to minimize their effects on the color gradient. We have therefore eliminated the 9 columns of superpixels on the western edge of Figure 11 where more rapid changes in the relative numbers of disk and halo stars are expected. Over the rest of the image the disk stars dominate and the contribution from halo stars to the V-I colors of each superpixel ought to be minimal.

The final correlation between $E(V-I)$ and $N(HI)$ obtained from our data is shown in Figure 12. Note that the points in this figure are not all independent, hence the apparent non-gaussian distribution. In order to compare this result to the values found for the Galaxy we need to convert our $E(V-I)$ values to $E(B-V)$. Assuming again that the extinction law in this part of M 31 is the same as that for solar neighbourhood of the Galaxy⁴, one

⁴This is a reasonable assumption according to Bouchet et al.

has $E(V-I_{Cousins}) = 1.60 \times E(B-V)$. Thus, including the 90% correction factor explained above, the correlation in Figure 12 implies:

$$\frac{N(HI)}{E(B-V)} = 1.45 \times 10^{22} \text{ atoms cm}^{-2} \text{ mag}^{-1}, \quad (1)$$

which is 3 times the canonical Galactic value of $4.8 \times 10^{21} \text{ atoms cm}^{-2} \text{ mag}^{-1}$ (Bohlin et al. 1978). We recall that the reddening we measure is only a lower limit to the total reddening through the disk of M 31, since some fraction of the stars we are using will be in front of the absorbing material, whereas the H I column refers to the entire line of sight through the galaxy. The value for $N(HI)/E(B-V)$ we give above is therefore an overestimate, and there will be more dust present on average than we have determined.

Our lower limit to $E(B-V)$ shows that, even in these sparse outer parts of M 31, the H I still contains a large amount of dust, indicative of a metallicity at least 1/3 of the value in the solar neighborhood if the dust/gas ratio is proportional to metallicity (e.g. Issa et al. (1990); Schmidt & Boller (1993); Bouchet et al. (1985)). An alternative to high dust/gas ratio or high metallicity could be that the region contains not only atomic, but also molecular hydrogen, with a distribution similar to that of H I. The dust we have detected would then correspond to both components of the gas, whereas our estimate of the gas column of course refers only to the atomic component.

6. The Bright Background Galaxies

Owing to confusion by overlapping star images in M 31, small galaxies can not reliably be identified for use as probes of obscuration in our image. However, there are quite a number of “large”, bright galaxies which appear in the image; they cover many pixels and are easily identified. We have therefore catalogued these objects by a detailed visual examination of each CCD chip and measured their magnitudes and colors. The identifications were independently made by two of us (J.C. and J.L.) and are considered extremely reliable. The number of these objects appearing in

(1985) who find similar laws in the visible and the infrared for the Galaxy and the two Magellanic Clouds in spite of large differences in metallicity.

various magnitude intervals over the entire field of all 7 CCD chips is as follows: $V < 19.5$, 66 objects; $19.5 < V < 20.5$, 193; $20.5 < V < 21.5$, 148; and, $21.5 < V < 22.5$, 147. The locations of these galaxies are shown in Figure 13 along with the contours of $\mathrm{N}(\mathrm{H}\mathrm{I})$. Note the striking lack of bright galaxies just in the region of the highest $\mathrm{H}\mathrm{I}$ contours in this figure.

6.1. Counts of the bright galaxies

The deficit of bright galaxies at high values of $\mathrm{N}(\mathrm{H}\mathrm{I})$ can be quantified by counting the number of galaxies with $V < 22.5$ in Figure 13 at various $\mathrm{H}\mathrm{I}$ contour intervals. The results are shown in Figure 14a. The data show a slight downward trend of the counts with increasing $\mathrm{N}(\mathrm{H}\mathrm{I})$; a linear regression through the points gives:

$$N_G = 0.725 - 1.6 \times \frac{N(\mathrm{H}\mathrm{I})}{10^{22} \mathrm{cm}^{-2}}, \quad (2)$$

in units of galaxies/superpixel, with a correlation coefficient 0.828. This relation can be converted into a relation between extinction and $\mathrm{N}(\mathrm{H}\mathrm{I})$ as follows: The differential luminosity function of galaxies at a given magnitude can be written as $N_G(m) = C \times 10^{\alpha m}$. The ratio of the counts $N_G(m)$ in one extinguished region (e.g. with extinction A_V mag) to those $N_{G0}(m)$ in a reference region at the same detection limit is then $N_G(m)/N_{G0}(m) = 10^{-\alpha A_V}$. Now $\alpha = 0.38$ (Arnouts et al. 1997) for galaxy counts in V over a similar range of magnitudes ($19 < V < 24$). Hence from $N(\mathrm{H}\mathrm{I}) = 0$ to 15×10^{20} , $N_G(m)/N_{G0}(m) = 0.67$ and so $A_V = 0.46$ mag. This yields $N(\mathrm{H}\mathrm{I})/A_V = 3.3 \times 10^{21}$, or $N(\mathrm{H}\mathrm{I})/E(B - V) = 1.0 \times 10^{22}$, to be compared with 4.8×10^{21} for our Galaxy. Thus the dust-to-atomic-gas ratio by this method is ≈ 0.5 Galactic, compared to the minimum value of $\gtrsim 0.33$ Galactic found from the stars. These results are therefore consistent, although the errors on the counts of the bright galaxies are of course much larger.

It is interesting to note that the decrease in large galaxy counts with increasing A_V which we have found in the outer parts of M31 is entirely consistent with the results of González et al. (1998), who applied a much more exhaustive analysis to fields of nearby galaxies imaged with the WFPC2 camera on the Hubble Space Telescope. Our equation 2 above can be re-written as

$N_G/N_{G0} = 1 - 0.81 \times A_V$, while the simulations shown in Figure 13 of González et al. (1998) can be parametrized by $N_G/N_{G0} = 1 - 0.77 \times A_V$ at least out to an $A_V \approx 1$, after accounting for the small excess reddening of $E(V - I) \approx 0.2$ which they determined from their data on NGC 4536. González et al. (1998) also found evidence for a contribution of high opacity clumps, at least in spiral arms.

Could the deficit in the distribution of bright galaxies at high values of $\mathrm{N}(\mathrm{H}\mathrm{I})$ shown in Figure 13 be merely a consequence of the known *clustering of galaxies* in the Universe? While this can not obviously be ruled out, we note that a two-fold conspiracy is required: First, the position of the “void” on the sky would have to correspond closely with the distribution of $\mathrm{N}(\mathrm{H}\mathrm{I})$; and second, the decrease in galaxy counts shown in Figure 14a would have to be just what would be predicted from the distinctly different analysis of González et al. (1998) on an entirely different galaxy.

6.2. Colors of the bright galaxies

Our data analysis also yields the colors of the bright galaxies. We have calculated histograms of the $V - I$ colors for all bright galaxies in each interval of $\mathrm{N}(\mathrm{H}\mathrm{I})$. The histograms show some outliers, perhaps a consequence of inaccurate photometry, so we have generally used the median colors instead of the means. If the means were used, we first truncated the histograms at 2σ . The results are shown in Figure 14b, from which we have to conclude that there is no evidence for reddening of the bright background galaxies, whereas the reddening of the stars was 0.15 mag for the same conditions. This result is actually consistent with the behavior of galaxy colors at faint magnitudes. The effective magnitude limit will shift at higher values of $\mathrm{N}(\mathrm{H}\mathrm{I})$ owing to the extinction. For instance, at $N(\mathrm{H}\mathrm{I}) = 1.5 \times 10^{21} \mathrm{cm}^{-2}$, $A_V \approx 0.4$, so the magnitude limit of $V < 22.5$ is actually shifted to $V < 22.1$. Of course it is precisely this shift which causes the decrease in the counts shown in Figure 14a. But this shift also accompanied by a change of *intrinsic* color of the background galaxies. From the data in the comparison field in Figure 6, and summarized in Table 1, we see that a shift in the magnitude limit from 22.5 to 22.1 leads to an average *blueing* of galaxies by $\Delta\langle V - I \rangle = -0.1$, just enough to compensate for the anticipated *reddening* of $\Delta\langle V - I \rangle = 0.15$ observed for the stars with

the same amount of extinction. We conclude that the absence of reddening with increasing $N(\text{HI})$ for the bright galaxies is consistent with the presence of significant amounts of dust mixed in with the gas.

7. Young Stars in the Outer Disk of M 31

A striking feature of the C–M diagram of Figure 8a is the presence of a vertical sequence of blue stars with $V - I \approx 0$, well separated from the Red Giant branch. Previously, Hodge (1988) and Davidge (1993) found blue stars in two different fields located at ~ 20 kpc from the center of M 31, but our field is larger and significantly further out in the disk and extends over a range of projected galactocentric distances from about 23 to 33 kpc. In Figure 15 we show the distribution of these stars plotted over the HI contours. There is a good correspondence of the number density of these stars with the HI column density. There are even some clusters visible. The few remaining blue objects e.g. in the extreme south-west corner are probably Galactic white dwarfs or quasars, which will cause a small contamination over the whole image of M 31.

A study of the C–M diagram of stars in a part of our field was carried out earlier by (Richer et al. 1990). However, their work refers to a region of low HI density located near the middle of our image on the East side, where few blue stars are to be found.

We find it somewhat surprising to have discovered evidence for star formation which is both ongoing and wide spread in the outer disk of M 31. According to the current view of the star formation process, molecular gas is therefore also expected to be present.

A discussion of the local conditions in this part of M 31 (gas disk surface density and velocity dispersion) in the context of stability thresholds and rates of star formation in galaxy disks (Kennicutt 1989; Elmegreen 1995) is hampered by the high inclination of M 31. The observed HI column density in this region is $N(\text{HI}) \approx 10^{21} \text{ HI atoms cm}^{-2}$, only about a factor of 4 below the column densities observed in the “star-forming ring” of M 31 at about 10 kpc galactocentric radius (Emerson 1974). Face-on values will be a factor of ≈ 4.4 smaller (for an inclination of 77°) if a uniform slab

model is assumed for the gas disk. The representative column densities in our outer disk field of M 31 are therefore about $2.3 \times 10^{20} \text{ HI atoms cm}^{-2}$. Owing to the high inclination, the determination of intrinsic gas velocity dispersion also suffers from averaging of gas cloud profiles along the line of sight. The calculation of a critical density is therefore uncertain, but it seems likely that the observed gas surface density is well below the threshold for forming very massive, ionizing stars. This is in agreement with our observations, since the young stars we have found do not seem to include stars more luminous than about B0.

Deep $\text{H}\alpha$ images of three actively-star-forming late-type spiral galaxies (NGC 628, NGC 1058, & NGC 6946) provide new evidence for massive star formation at galactocentric radial distances up to $\approx 2 \times R_{25}$ (Ferguson et al. 1998a,b). Our results on M 31 show that ongoing star formation activity can also take place in the outer parts of earlier-type galaxies, although the stars being formed are generally of lower mass.

8. Conclusions

We have presented evidence for the existence of appreciable amounts of dust well mixed with the atomic gas in the far outer regions of M 31, in an area at a galactocentric radius of $\approx 116'$, or $\approx 1.2 \times R_{25}$. The dust-to-atomic-gas ratio is $\gtrsim 1/3$ of the Galactic value in the solar neighborhood. These results refer not to isolated positions, but to large areas of size ~ 20 kpc 2 or more in the outer disk of this galaxy. Dust is made of heavy elements; if primordial gas is expected to be lacking in heavy elements (and therefore contains no dust), then the extended HI gas in the outer parts of M 31 is not primordial.

High values of metallicity in the outer disk of M 31 are not completely unexpected. Jacoby & Ford (1986) measured an oxygen abundance $O/H = 3.2 \times 10^{-4}$ in an HII region 17 kpc from the center of M 31, and a value of 1.2×10^{-4} in a planetary nebula at 33 kpc projected radius, but this object has halo kinematics. In our Galaxy, De Geus et al. (1993) and Digel et al. (1994) have detected CO emission from gas at a kinematic distance of 28 kpc. This shows that heavy elements are present in the Galaxy almost at the edge of the HI disk (kinematic radius ~ 30 kpc). Ferguson et

al. (1998a) also report metallicities of 0.10 - 0.15 solar in HII regions in the outer parts of several late-type spirals. However, these detections refer to isolated positions where peculiar local conditions may occur; our result on M 31 refers to the outer disk gas in general.

We have also found evidence for recent star formation in the outer parts of M 31. These young stars have the signatures of B stars and appear both in clusters and in isolation. Their presence points to the existence of molecular gas in the outer disk of M 31. The amount of molecular gas can not be directly determined from our observations, and if it is very cold ($T_k \lesssim 5$ K) and/or of modest density ($\lesssim 300$ H₂ molecules cm⁻²), detecting photon emission from it will be very difficult. As an order-of-magnitude estimate, we note that the addition of a column N(H₂) of molecular gas equivalent to the observed column N(H I) of atomic gas would reduce our observed dust-to-atomic-gas ratio of $\gtrsim 1/3$ to a dust-to-*total-gas* ratio of $\gtrsim 1/9$, a value more in agreement with the low metallicities in the outer parts of disk galaxies reported by Ferguson et al. (1998a).

Finally, we have found a suggestion in our data that the ISM in the outer disk of M 31 is clumpy on length scales smaller than about 200 pc. While this result may be well-known for the ISM in the inner parts of galaxies, our data provides the first indication that the gas in the faint outer disks of galaxies is similarly clumpy. A higher-resolution map of the H I distribution in this area with e.g. the VLA would provide the means to examine the correspondence of gas, dust, and young stars in these outer regions of M 31 in significantly more detail.

The observations were collected at the Canada-France-Hawaii Telescope at Mauna Kea. We thank Gerard Luppino of the University of Hawaii for the loan of the UH8K CCD mosaic camera which made the present observations possible, and the Directors of the Canada-France-Hawaii Telescope and Space Telescope Science Institute for financial support which facilitated the work on this paper. The blank field data were kindly provided by M. Crézé and A. Robin. Helpful comments on earlier drafts of the paper were made by Nino Panagia and Ken Freeman.

REFERENCES

Arnouts, S., de Lapparent, V., Mathez, G., Mazure, A., Mellier, Y., Bertin, E., Kruszewski, A. 1997, *A&AS*, 124, 163

Bertin E., & Arnouts, S. 1996, *A&AS*, 117, 393

Bohlin, R.C., Savage, B.D., & Drake, J.F. 1978, *ApJ*, 224, 132

Bouchet P., Lequeux J., Maurice E., Prévot L., & Prévot-Burnichon M.-L. 1985, *A&A*, 149, 330

Boulade, O., Vigroux, L.G., Charlot, X., Borgeaud, P., Carton, P.-H., de Kat, J., Roussé, J.Y., Mellier, Y., Gigan, P., Crampton, D., Morbey, C.L. 1998, *Proc. SPIE*, 3355, 614

Cuillandre, J.-C. 2001, *A&A* (in preparation)

Davidge T.J. 1993, *ApJ*, 409, 190

De Geus E.J., Vogel S.N., Digel S.W., Gruendl R.A. 1993, *ApJ*, 413, L97

Digel S., de Geus E.J., & Thaddeus P. 1994, *ApJ*, 422, 92

Elmegreen, B.G. 1995, *MNRAS*, 275, 944

Emerson, D.T. 1974, *MNRAS*, 169, 607

Feast M. 1999, in “The Stellar Content of Nearby Galaxies”, IAU Symposium 192, ed. P. Whitelock & R. Cannon, Astronomical Society of the Pacific, p. 51

Ferguson, A.M.N., Gallagher, J.S., Wyse, R.F.G. 1998, *AJ*, 116, 673

Ferguson, A.M.N., Wyse, R.F.G., Gallagher, J.S., Hunter, D.A. 1998, *ApJ*, 506, L19

González R.A., Allen R.J., Dirsch B., Ferguson H.C., Calzetti D., Panagia N. 1998, *ApJ*, 506, 152

Hodge, P.W. 1974, *ApJ*, 192, 21

Hodge P., Lee M.G., Mateo M. 1988, *ApJ*, 324, 172

Innanen K.A., Kamper K.W., Papp K.A., & van den Bergh S. 1982, *ApJ*, 254, 515

Issa, M.R., MacLaren, I., & Wolfendale, A.W. 1990, *A&A*, 236, 237

Jacoby G.H., & Ford H.C. 1986, *ApJ*, 304, 490

Kennicutt, R.C. 1989, *ApJ*, 344, 685

Landolt A.U. 1992, *AJ*, 104, 340

Lequeux, J. 1994, *A&A*, 287, 368

Lequeux J., Dantel-Fort M., & Fort, B. 1995, *A&A*, 296, L13

MacGillivray, H.T. 1975, *MNRAS*, 170, 241

Majewski, S.R., Kron, R.G., Koo, D.C., & Bereshady, M.A. 1994, *PASP*, 106, 1258

Newton K., & Emerson D.T. 1977, *MNRAS*, 181, 573

Richer H.B., Crabtree D.R., & Pritchett C.J. 1990, *ApJ*, 355, 448

Sandage, A., & Tammann, G.A. 1981, “A Revised Shapley-Ames Catalog of Bright Galaxies”, Carnegie Institute of Washington Publication 635

Savage, B.D., & Mathis, J.S. 1979, *ARA&A*, 17, 73

Schmidt, K.-H., & Boller, T. 1993, *Astron. Nachr.*, 314, 361

Walterbos R.A.M., & Kennicutt, R.C. Jr. 1988, *A&A*, 198, 61

Zaritsky D. 1994, *AJ*, 108, 1619

TABLE 1
COUNTS AND COLORS OF GALAXIES IN THE SA 57 BLANK FIELD.

V magnitude	Counts	$\langle V - I \rangle$ Colors
$V < 22.1$	185	1.1
$V < 22.5$	280	1.2
$V < 24.75$	2025	1.0

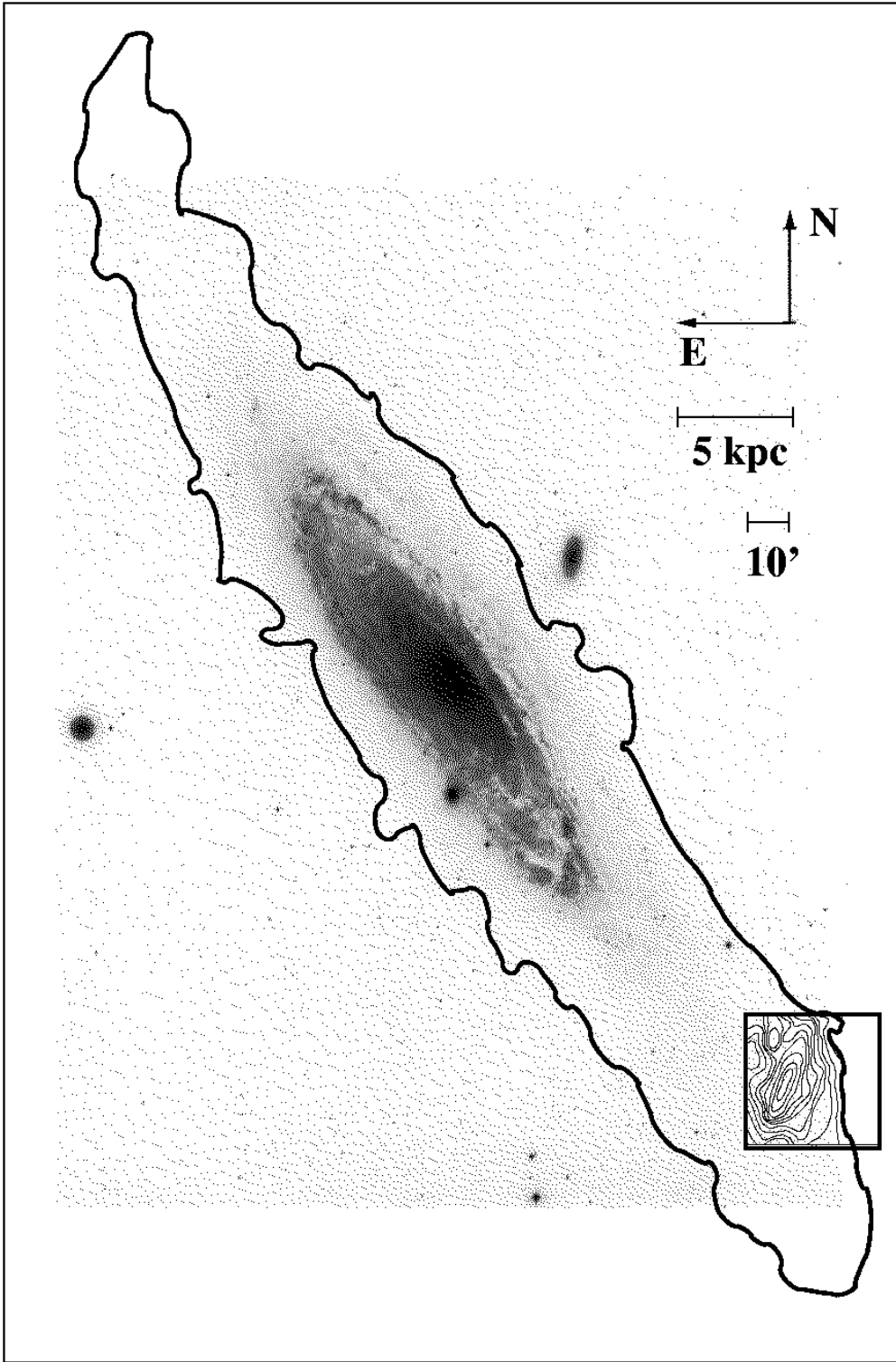


Fig. 1.— Sketch of the relation of the observed $28' \times 28'$ UH8K field (square box at lower right) to the optical image of M31 (Sandage & Tammann 1981). Also shown is the large-scale HI emission extending over 5° , (thick contour, at $\approx 8 \times 10^{19}$ atoms cm^{-2}), and the higher-resolution HI map (thin contours within the UH8K field, see Figure 11 for contour values), from Emerson (1974) and Newton & Emerson (1977).

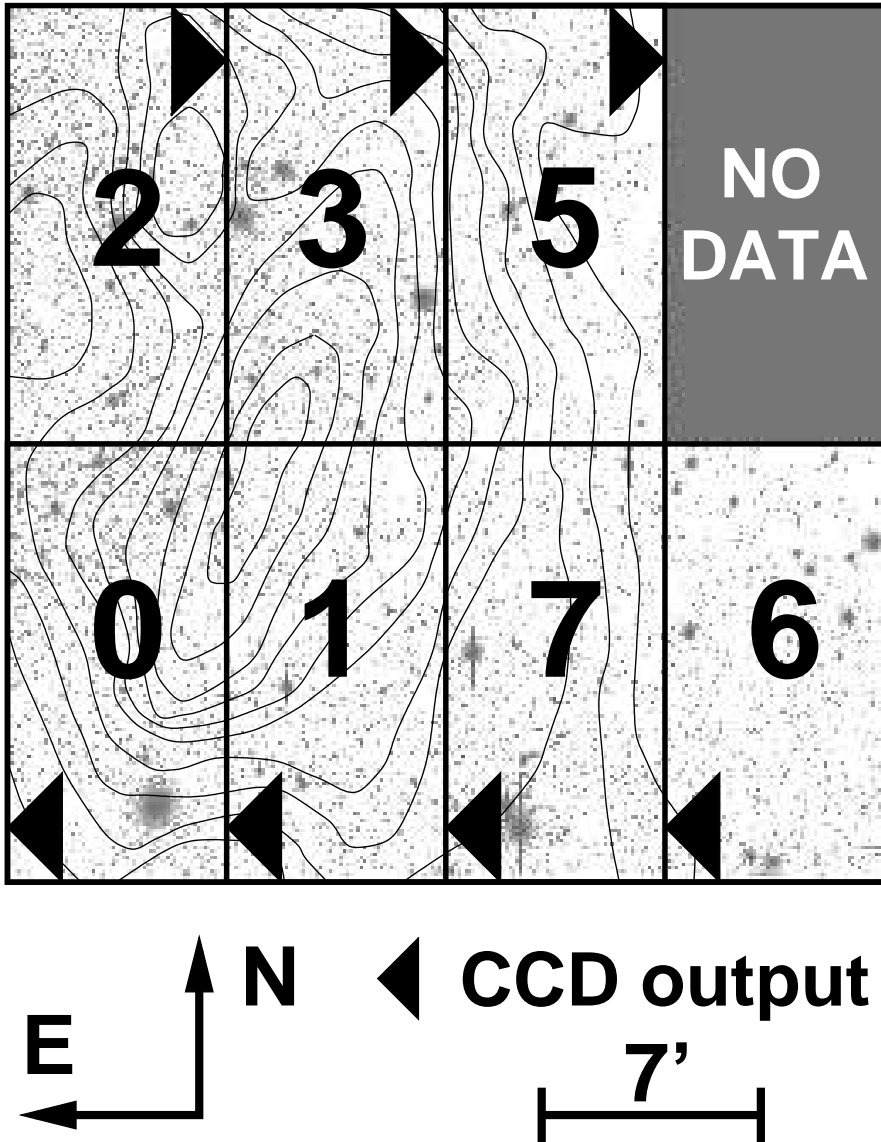


Fig. 2.— Sketch of the full UH8K field showing the location of the 8 CCD chips which make up the mosaic. CCD4 has been ignored in this paper. The arrowheads show the readout directions for each chip. Note that there are very few bright Galactic stars contaminating this field.

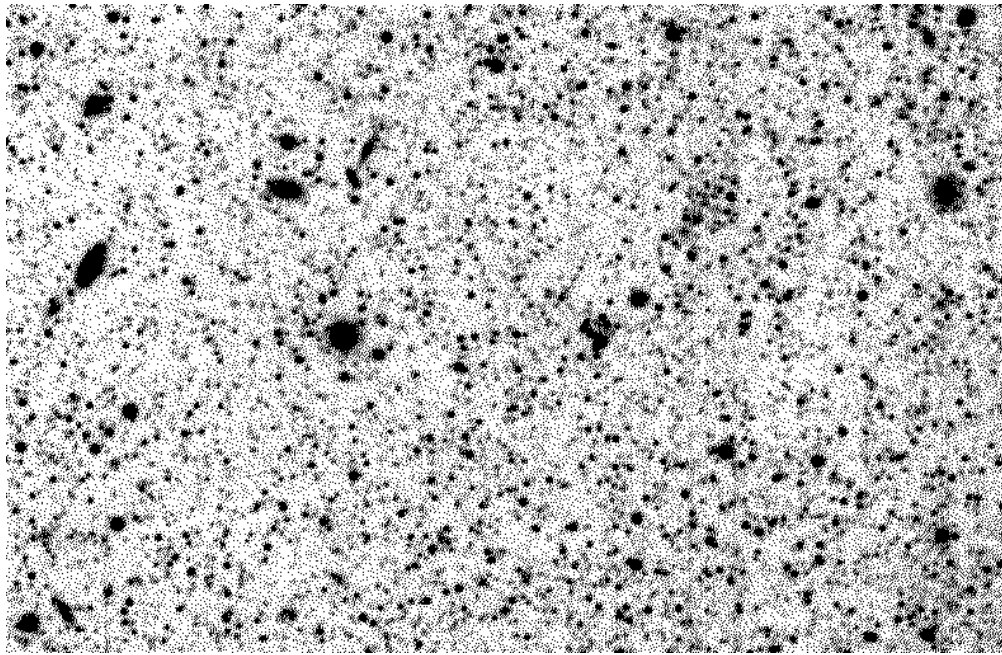


Fig. 3.— A portion of the final averaged V image in CCD3. This sub-image is 700×500 pixels = $2.40' \times 1.72'$ in size and is oriented on this page such that north is up and east is to the left.

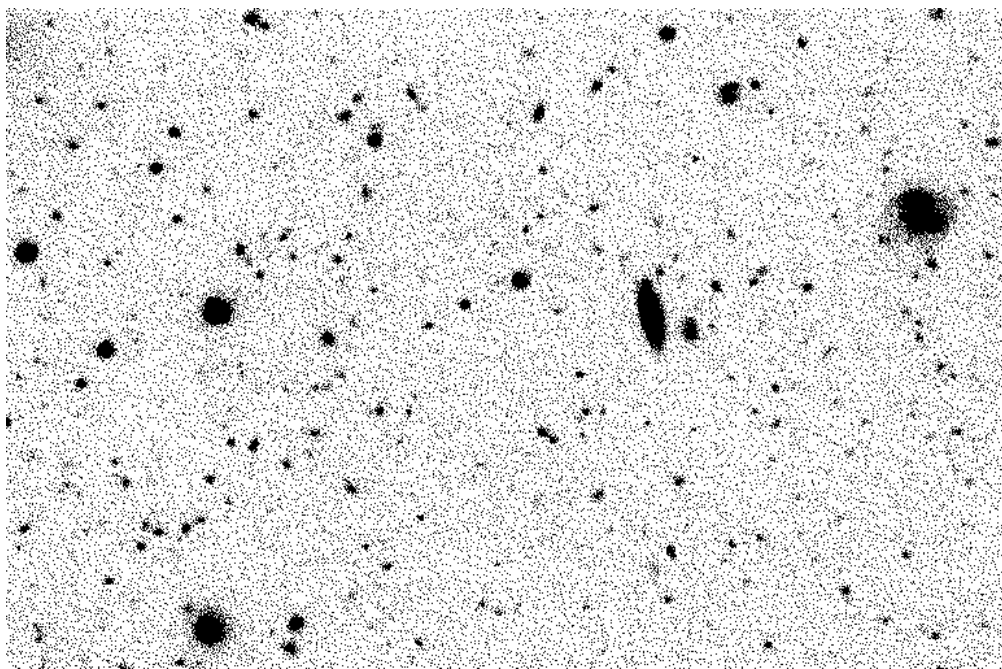


Fig. 4.— A portion of the final averaged V image in SA 57. This sub-image is 700×500 pixels = $2.40' \times 1.72'$ in size and is oriented on this page such that north is up and east is to the left.

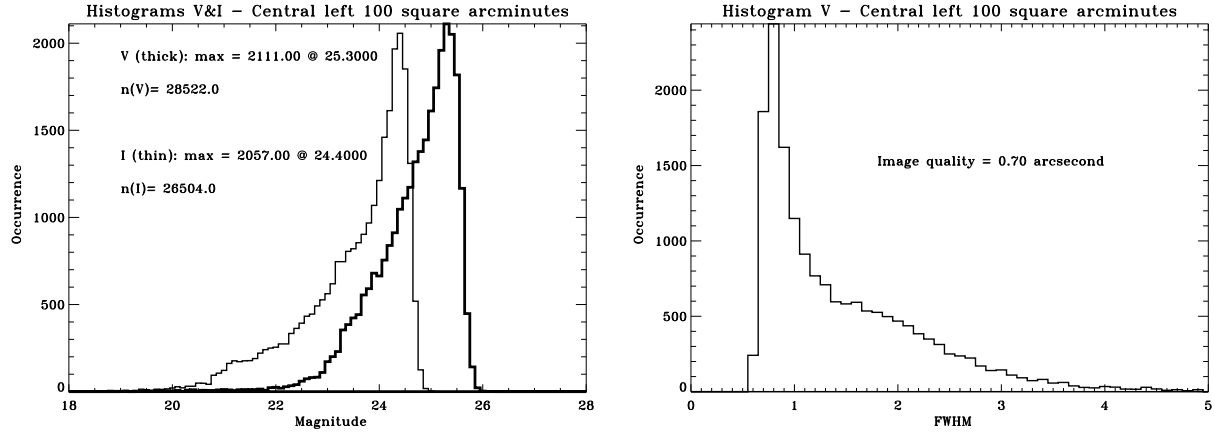


Fig. 5.— The histograms for all objects on a sub-field of 100 arcmin² covering one of the CCD chips. a) (left panel) Histograms of V and I. The smooth rise and rapid drop illustrate the high degree of completeness of our sample, to $V < 25.4$, $I < 24.4$. b) (right panel) Histogram of object sizes (FWHM).

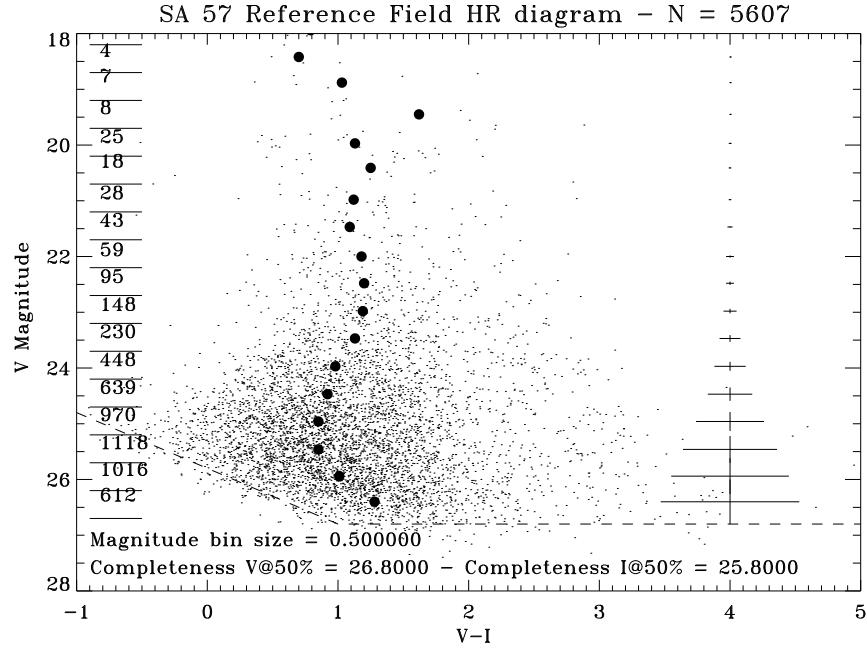


Fig. 6.— Color–Magnitude diagram for galaxies (objects with FWHM $> 1.5''$) in CCD3 on the “blank” field SA 57 near the Galactic North Pole. The area covered on the sky is $7.03' \times 14.06'$.

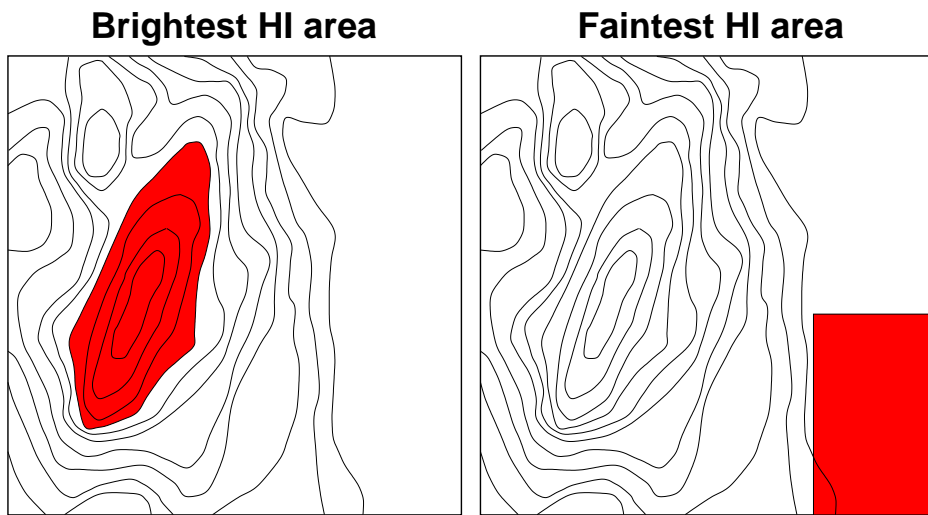


Fig. 7.— The areas defined on the field in regions which are bright in H I (left panel) and faint in H I (right panel). The areas are the same, 70 arcmin². Contour levels are given in Figure 11; the H I-bright area in the left panel includes contours at and above $N(\text{H I}) = 1.1 \times 10^{21} \text{ H I atoms cm}^{-2}$.

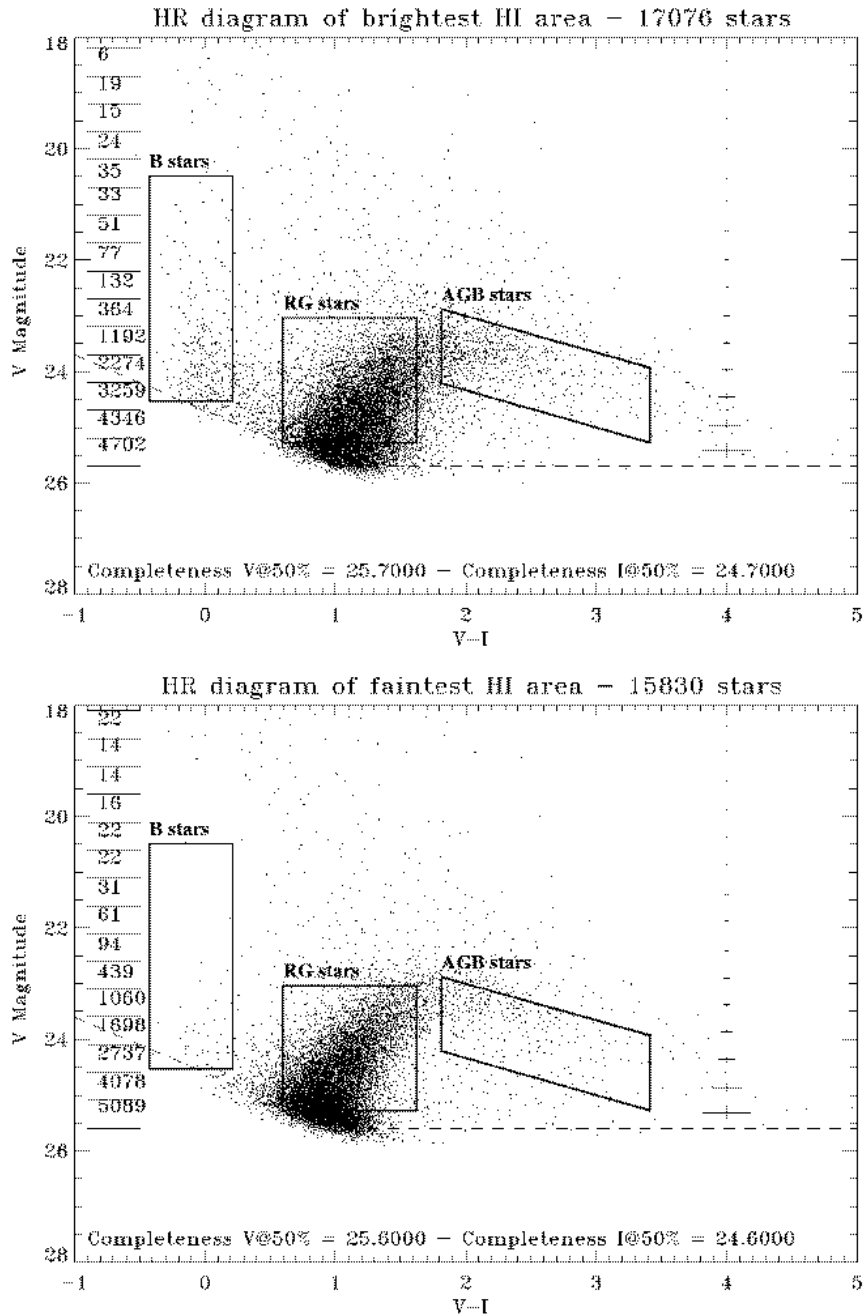


Fig. 8.— The V vs. V-I color-magnitude diagrams for objects classified as stars: a) (upper panel) in the brightest HI areas of the image, as shown in the inset; and, b) (lower panel) in the south-west part of our field, well away from the bright HI contours. In both cases the sub-fields are 70 arcmin^2 in area, and contain nearly the same number of stars ($\approx 16,000$). The boxes in these figures delineate areas of the C-M diagram populated by stars in M31 of different types; B-stars, Red Giants (RG), and Asymptotic Giant Branch (AGB) stars. Note the shift of the data points downwards and to the right in panel (a) compared to panel (b), a consequence of extinction and reddening by dust mixed in with the HI.

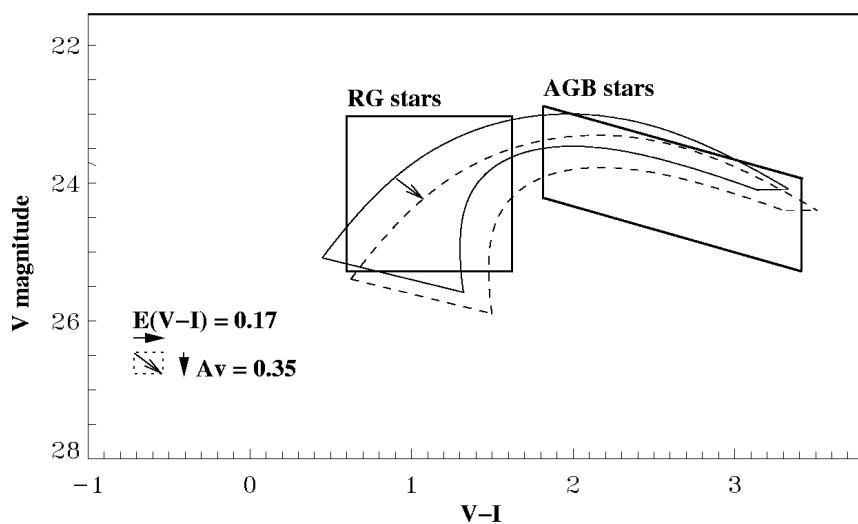


Fig. 9.— Sketch showing the shift of the data from Figure 8b to Figure 8a as a result of extinction and reddening. Our rough derivation of the values of the shifts in the two coordinates is shown on the Figure.

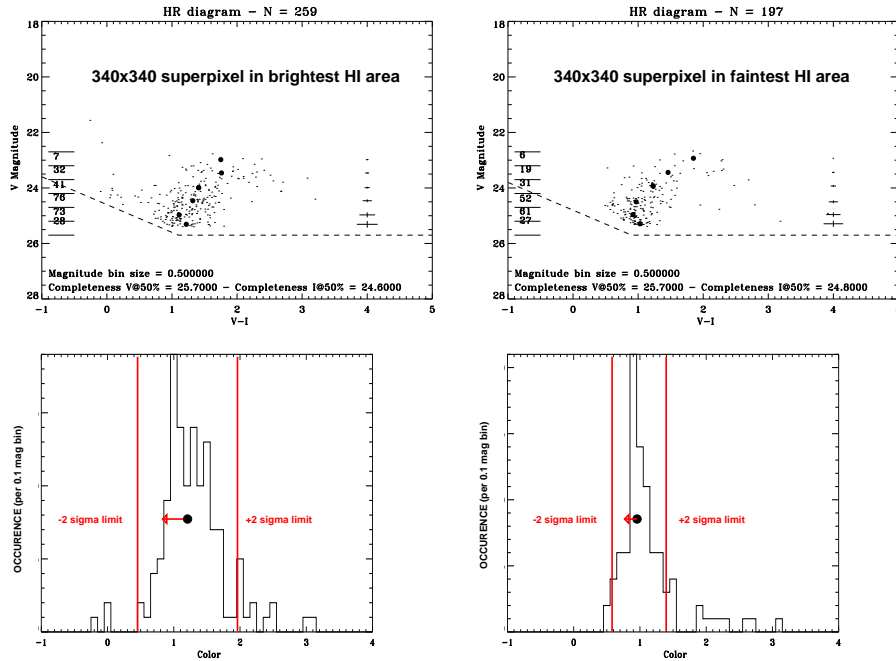


Fig. 10.— C–M diagrams for two representative superpixels, one in an HI-rich area (upper left) and one in an HI-poor area (upper right). The lower panels are the corresponding histograms from which we compute the mean V–I colors, indicated by the large dot in the middle of the figure. The horizontal arrow anchored to this dot shows the 1σ dispersion.

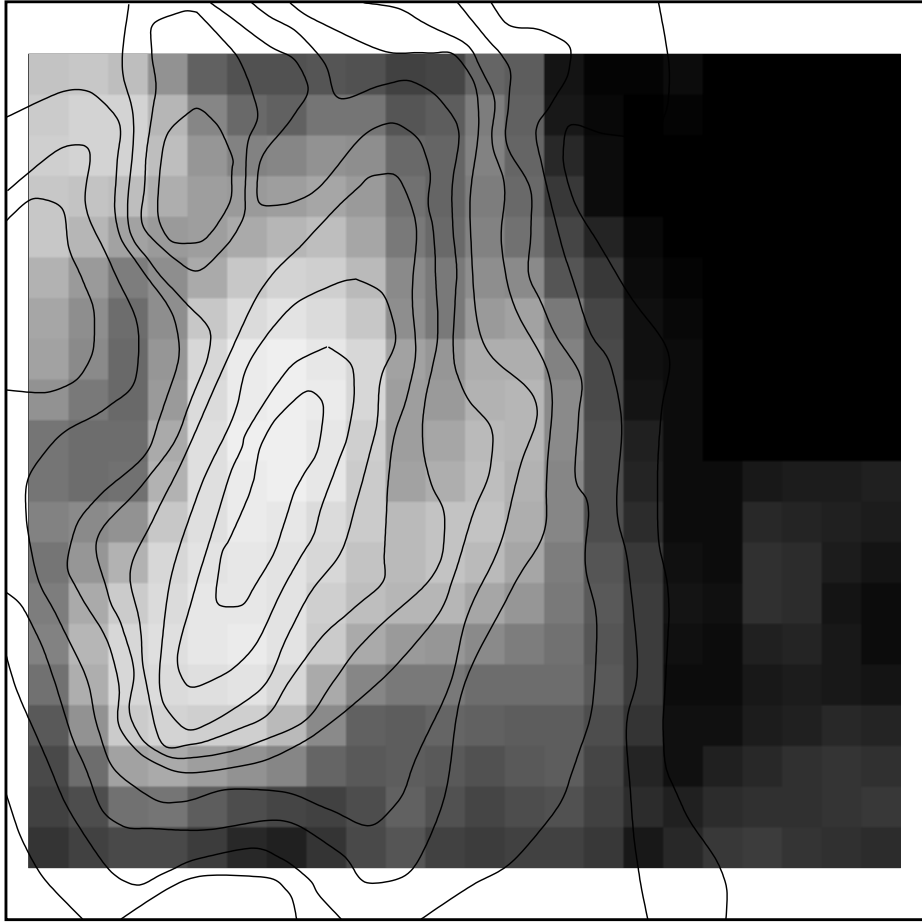


Fig. 11.— Map of the mean color $\langle V - I \rangle$ of stars in the field (grey scale) compared to the column density of HI (contours). The field center is at $\alpha(1950) = 00h 33m 21.4s$, $\delta(1950) = 39^\circ 32' 21''$. The color map is represented in “superpixels”, but has been smoothed to 3×5 superpixels in order to more closely correspond with the HI resolution. The grey scale goes from $\langle V - I \rangle = 1.05$ (dark) to $\langle V - I \rangle = 1.26$ (white) on a linear scale. The HI map is from Newton & Emerson (1977) with a resolution of $3.6' \text{ EW} \times 5.8' \text{ NS}$ FWHM, and has here been corrected for their primary beam attenuation. The UH8K mosaic was rotated $+3.6^\circ$ (east through north) to conform to the N–S orientation of the HI map. The HI contours are drawn at levels of 2 through 18 in steps of 2, plus contours at 13 and 19, in units of $7.7 \times 10^{19} \text{ atoms cm}^{-2}$. Note the good correlation between reddening and the column density of HI.

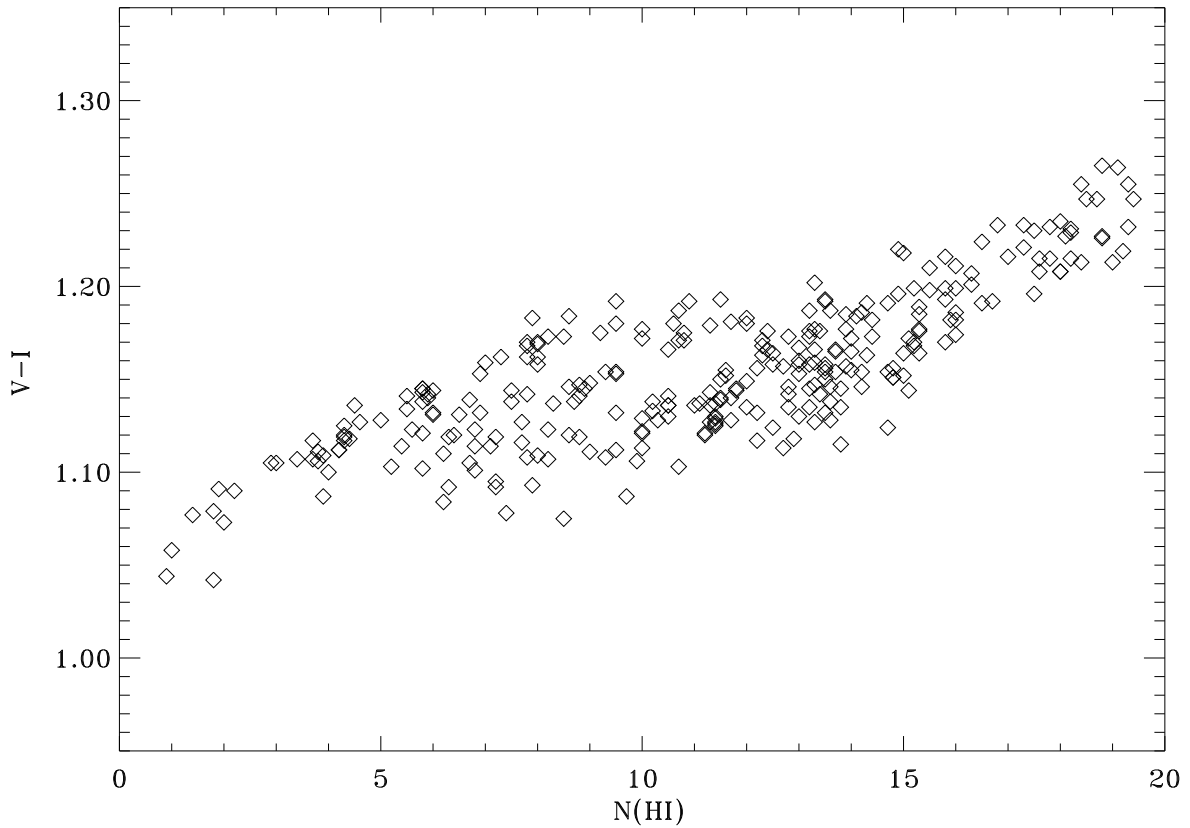


Fig. 12.— The relation between the mean color $\langle V - I \rangle$ (mag) of stars and the column density of HI (in units of 7.7×10^{19} atoms cm^{-2}) corresponding to the image of Figure 11. The 9 columns of superpixels at the right of Fig. 11 have not been used to build this correlation in order to reduce the effects of contamination by bluer halo stars. We have also checked that the Galactic hydrogen as depicted indirectly by the IRAS 100 μm map does not contaminate this diagram. Note that the points in this figure are not independent, hence the non-gaussian distribution.

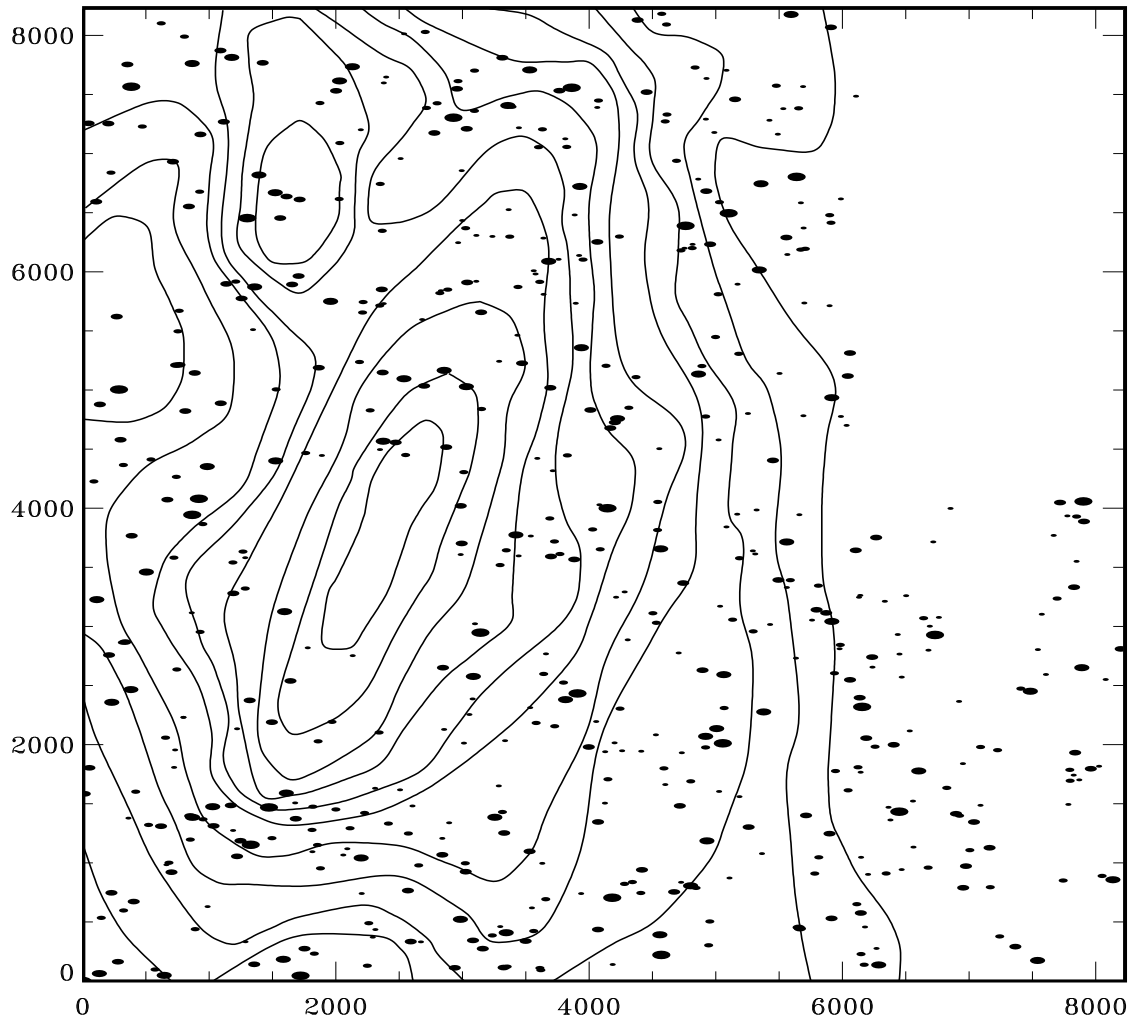


Fig. 13.— The distribution of “large” bright background galaxies over the image as identified from a visual inspection of each CCD chip. The largest symbol corresponds to galaxies with $V < 18.5$. The remaining 4 smaller symbols indicate galaxy magnitudes ranging from 19 ± 0.5 mag (larger symbol) to 22 ± 0.5 mag (smallest symbol). The contours are $N(\text{HI})$ as in Figure 11.

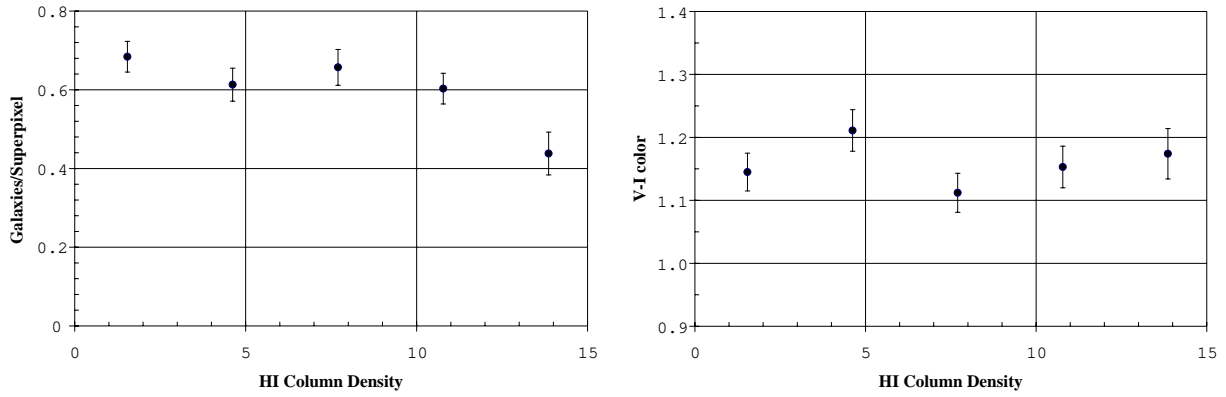


Fig. 14.— a) (left panel) The surface density of bright background galaxies with $V < 22.5$ in the image at different levels of atomic gas surface density $N(\text{H I})$. The units of N_G are galaxies/superspixel; a superspixel is 1.36 arcmin^2 . b) (right panel) The colors of bright background galaxies in the image at different $N(\text{H I})$ levels. The units of $N(\text{H I})$ in both panels are $1.0 \times 10^{20} \text{ atoms cm}^{-2}$.

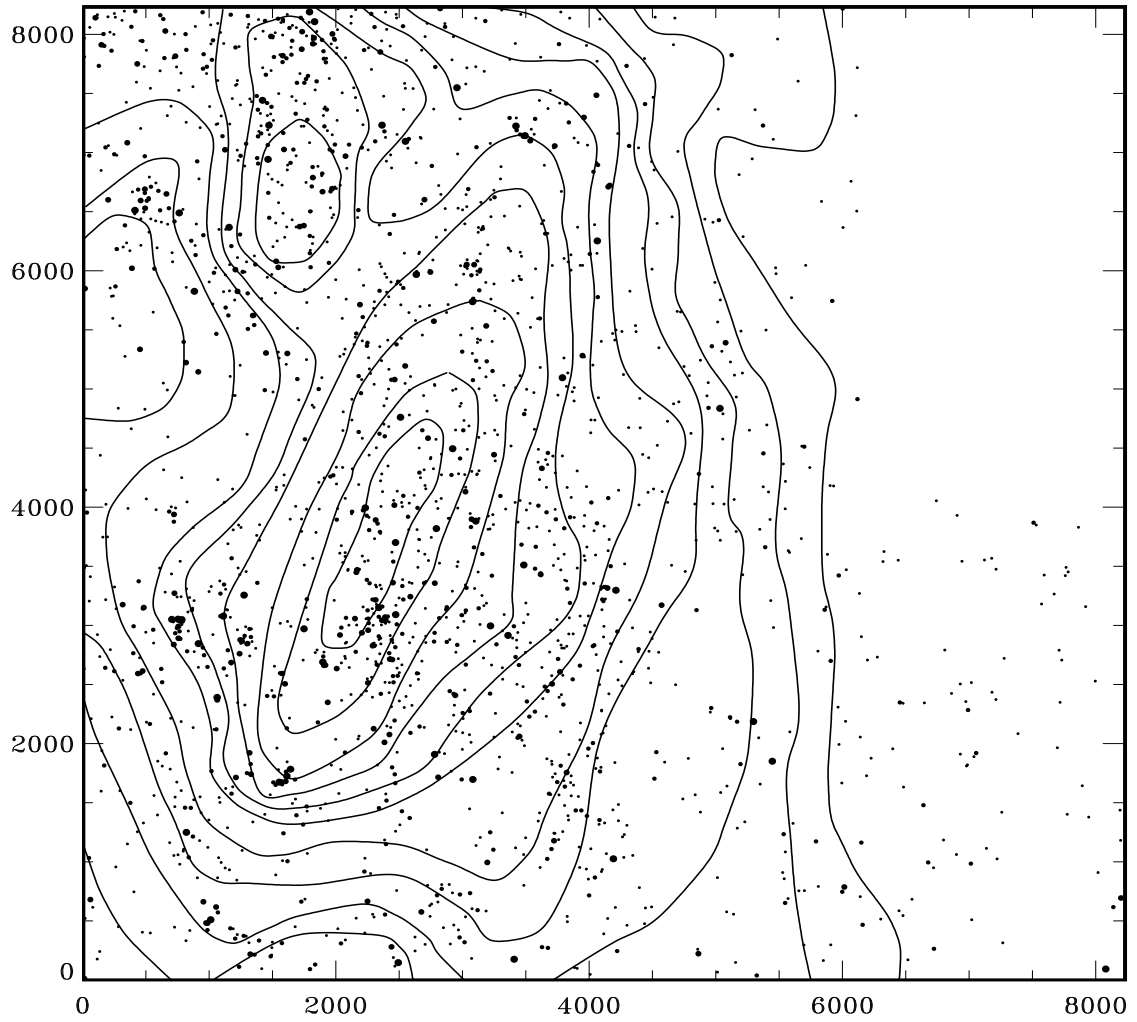


Fig. 15.— The distribution of the blue stars over the extreme outer disk of M31. The symbols show the locations of stars in the range $20.5 < V < 24.5$ with colors $-0.5 < V - I < 0.2$. Brighter stars have larger symbols, in 4 steps of 1 mag. The contours of HI column density are superimposed as for Figure 11. There is some contamination by quasars and Galactic white dwarfs, which are visible e.g. in the halo field at the extreme south-west of the image.